SCIENCE CHINA
Chemistry

•ARTICLES•

March 2019 Vol.62 No.3: 378–384
https://doi.org/10.1007/s11426-018-9375-2

Trimetallic Au@PdPt core-shell nanoparticles with ultrathin PdPt skin as highly stable electrocatalysts for the oxygen reduction reaction in acid solution

Xiaokun Li[1], Chunmei Zhang[1,2], Cheng Du[1,3], Zhihua Zhuang[1,3], Fuqin Zheng[1,2], Ping Li[1,3], Ziwei Zhang[1,3] & Wei Chen[1,3*]

[1]*State Key Laboratory of Electroanalytical Chemistry, Changchun Institute of Applied Chemistry, Chinese Academy of Sciences, Changchun 130022, China;*
[2]*University of Chinese Academy of Sciences, Beijing 100039, China;*
[3]*University of Science and Technology of China, Hefei 230026, China*

Received August 9, 2018; accepted October 25, 2018; published online January 24, 2019

To design efficient and low-cost core-shell electrocatalysts with an ultrathin platinum shell, the balance between platinum dosage and durability in acid solution is of great importance. In the present work, trimetallic Au@PdPt core-shell nanoparticles (NPs) with Pd/Pt molar ratios ranging from 0.31:1 to 4.20:1 were synthesized based on the Au catalytic reduction strategy and the subsequent metallic replacement reaction. When the Pd/Pt molar ratio is 1.19:1 (designated as Au@$Pd_{1.19}Pt_1$ NPs), the superior electrochemical activity and stability were achieved for oxygen reduction reaction (ORR) in acid solution. Especially, the specific and mass activities of Au@$Pd_{1.19}Pt_1$ NPs are 1.31 and 6.09 times higher than those of commercial Pt/C catalyst. In addition, the Au@$Pd_{1.19}Pt_1$ NPs presented a good durability in acid solution. After 3000 potential cycles between 0.1 and 0.7 V (vs. Ag/AgCl), the oxygen reduction activity is almost unchanged. This study provides a simple strategy to synthesize high-performance trimetallic ORR electrocatalyst for fuel cells.

electrocatalyst, core-shell, platinum, oxygen reduction reaction, nanoparticle, fuel cell

Citation: Li X, Zhang C, Du C, Zhuang Z, Zheng F, Li P, Zhang Z, Chen W. Trimetallic Au@PdPt core-shell nanoparticles with ultrathin PdPt skin as highly stable electrocatalysts for the oxygen reduction reaction in acid solution. *Sci China Chem*, 2019, 62: 378–384, https://doi.org/10.1007/s11426-018-9375-2

1 Introduction

As the best electrocatalyst, platinum (Pt) and Pt-based nanomaterials have been widely used in fuel cells, such as proton exchange membrane fuel cells (PEMFCs) [1,2]. However, in the acid electrolyte, the low pH presents a highly corrosive effect on Pt-based materials on the cathode of PEMFCs, which can make Pt electrocatalysts easily dissolve in the solution under operating conditions [3–5]. Therefore, how to enhance the stability of Pt-based electrocatalysts is a big challenge for the commercialization of fuel cells [6]. Meanwhile, since Pt element is scarce and expensive, reducing Pt dosage is also a special consideration on the design of electrocatalysts. Based on these purposes, novel electrocatalysts with excellent catalytic performance have been explored by different strategies, including introducing other metals into Pt-based materials or using non-precious and abundant metals to replace Pt [1], changing the surface morphology and size for the improvement of electrochemical activity [7], designing monoatomic-layer Pt-shell nanostructures to lower the platinum content [8–11], and so on.

*Corresponding author (email: weichen@ciac.ac.cn)

Among these advanced materials, bimetallic/trimetallic nanostructures have attracted much attention [12–20]. For example, in Au-Pt composites, Au can increase the stability of catalysts by adjusting the electronic structure of Pt and lowering the d band center, which can increase the Pt oxidation potential and active oxygen species [21–24]. Meanwhile, various Pt-Pd nanomaterials exhibited enhanced electrochemical activities for oxygen reduction [25,26]. For example, for a core-shell structure with Pd core and a monolayer-thick Pt shell, Pt shell can be protected by loss of Pd in the oxygen reduction reaction (ORR) at the cathode of fuel cells in acid electrolyte [27]. Furthermore, with incorporating Au into Pd-Pt nanostructures, Au can substantially enhanced the ORR catalytic performance by improving the durability of the Au-Pd-Pt nanostructures [28,29]. Therefore, introducing Au and/or Pd into the Pt-based catalysts is an effective means to improve the durability of the electrocatalysts and enhance their electrocatalytic properties [30,31].

Recently, we have synthesized a type of Au@Pt core-shell nanoelectrocatalyst with self-controlled quasi-monolayer Pt skin using a Au catalytic reduction strategy [32]. The fabricated nanostructure showed high catalytic performances for the ORR and methanol oxidation reaction in alkaline solution. In the present work, based on the similar synthetic strategy, Pd is introduced into the synthetic process, and the trimetallic Au@PdPt core-shell nanoparticles (NPs) with a Au core and an ultrathin PdPt shell (up to about 2.6 atomic layers) were successfully obtained. In this interesting nanostructure, Pd acts as a protector for the Pt shell in acidic environment, which can compensate the corrosion effect of high oxygen content to ultrathin Pt surface in cathodic reaction. The synthesized Au@PdPt NPs presented higher ORR electrocatalytic activity and stability than Au@Pt NPs with Pt-skin surface obtained by our synthesis strategy.

2 Experimental

2.1 Materials and characterization

Potassium tetrachloroplatinate(II) (K_2PtCl_4), palladium chloride ($PdCl_2$) and hydrogen tetrachloroaurate(Ⅲ) trihydrate ($HAuCl_4•3H_2O$) were obtained from Sigma-Aldrich (USA). HEPES (4-(2-hydroxyethyl)-1-piperazineethanesulfonic acid) was purchased from Dingguo Biotechnology Co. Ltd. (Beijing, China). Other analytical chemicals were obtained from Beijing Chemical Reagents Co. Ltd. (Beijing, China). Milli-Q water (18.2 MΩ cm) was used in all experiments.

The transmission electron microscopy (TEM, Hitachi H-600, Japan) images were measured to study the morphology and size of the nanostructures. The more precise analysis for the products was carried out by a JEM-2010 (HR) microscope (JEOL, Japan) with operation at 200 kV, including high-resolution TEM images, high-angle annular dark-field scanning transmission electron microscopy (HAADF-STEM) images, the energy-dispersive X-ray spectroscopy (EDX) and elemental mapping. Powder X-ray diffraction (XRD) patterns for the crystal surface analysis of particles were recorded on a X-ray diffractometer (Bruker D8 Avance, Germany) with a Cu Kα radiation source (λ=1.54 Å) between 2θ from 10° to 80°. The X-ray photoelectron spectroscopy (XPS) measurements for the element valence state analysis of the products were performed on a VG Thermo spectrometer (ESCALAB 250, USA) with operation at 120 W and pass energy mode at 100 eV. The inductively coupled plasma atomic emission spectrum (ICP-AES) was used for the composition analysis of the products by a plasma emission spectrometer (Thermo iCAP 6300, USA).

2.2 Synthesis of trimetallic Au@PdPt core-shell nanoparticles with PdPt-skin surface (Au@PdPt NPs)

The information of the used chemicals is included in the Supporting Information online. Au nanoparticles (Au NPs) capped by citrates were firstly synthesized [33,34]. The Au NPs were concentrated by centrifugation and stored at room temperature. In the synthesis process, the stock solution of Au NPs was added to aqueous HEPES buffer (pH 7.5) to obtain a mixture (denoted as HEPES-Au-NPs). After a 5-min incubation, various volumes of Pd^{2+} ion stock solutions (0.01 M Pd^{2+} ions in the same concentration of HCl solution) were injected into the HEPES-Au-NPs to obtain a series of reaction solutions, in which the final concentrations of Au NPs and HEPES are 4.0 nM and 15 mM, and the concentrations of Pd^{2+} ions are 60, 100, 300 and 600 μM, respectively. The reaction solutions were stirred sufficiently and then incubated for 2 h at room temperature. Subsequently, various volumes of 0.01 M Pt^{2+} ion stock solution (in the same concentration of HCl solution) were introduced into these mixtures and incubated overnight at room temperature. These reaction solutions were centrifuged three times to remove excessive metal ions and then the Au@PdPt NPs with different Pd/Pt ratios were obtained. For comparison, Au@Pt (without Pd added) and Au@Pd (without Pt added) core-shell NPs were also synthesized according to the Au catalytic reduction strategy. The synthesized materials were characterized by various techniques (see Supporting Information online).

2.3 Electrochemical measurements

Electrochemical experiments were measured by an electrochemical workstation (CHI 750D) at room temperature. In a three-electrode cell system, the working, reference and counter electrodes are a rotating classy carbon disk electrode

(5 mm in diameter), an Ag/AgCl (saturated KCl) electrode and a platinum wire, respectively. 0.1 M $HClO_4$ solution was used as electrolyte. In the experimental procedure, the working electrode coated with the catalyst was prepared by dropping 3.0 mg mL^{-1} catalyst inks with 0.5% Nafion (10 μL) on the cleaned rotating disk electrode (RDE) surface followed by evaporation. For comparison, the catalytic performance of commercial Pd/C catalyst was also studied (see the Supporting Information online for other structural characterizations).

3 Results and discussion

3.1 The synthesis mechanism of Au@PdPt core@shell nanoparticles

In the previous work, we have developed a Au catalytic reduction strategy to synthesize a self-controlled Pt-monolayer shell on Au core [32]. Based on the Au catalysis, piperazine derivative (for instance HEPES) could reduce Pt^{2+} ions to Pt atoms and then form Pt skin surface on Au substrate. Since palladium is also a noble metal, we hypothesize that Pd^{2+} ions can also be reduced to Pd atoms and a Pd shell on Au core can be obtained based on this synthesis strategy. In the synthesis process, Pt^{2+} ions were added into the reaction system after the addition of Pd^{2+} ions for ensuring more Pd content in PdPt shell, because palladium was used as a protector to resist the corrosion of PtPd shell in the acid solution. With addition of sufficient Pd^{2+} ions in the reaction solution, enough Pd atoms can be formed on the surface of Au core, and therefore only limited Pt^{2+} can be reduced by HEPES based on the Au catalysis principle. Considering that Pt is more inert than Pd, there may mainly be a metallic replacement reaction between Pt^{2+} ions in the solution and the deposited Pd atoms on Au core surface. Therefore, the formation of PdPt shell on Au core includes the originally formed Pd shell due to the Au catalytic reduction effect and the subsequent metallic replacement reaction between Pt^{2+} ions and Pd atoms.

3.2 Characterization of the trimetallic Au@PdPt core@shell nanoparticles

To study the influence of the added Pd amount on the final content of Pt in the PdPt shell, elemental contents in the Au@PdPt NPs prepared from different Pd/Pt ratios and Au@Pt NPs were determined by inductively coupled plasma atomic emission spectrum (ICP-AES), as shown in Table S1 (Supporting Information online). In the absence of Pd^{2+} ions, the molar ratio of Pt/Au in Au@Pt NPs is 8.36%, i.e. approximately 1.22 Pt layers were formed on the Au core (see Supporting Information online for details). Next, the four samples of Au@PdPt NPs with more than a single Pt layer were studied. With adding a small amount of Pd^{2+} (such as 60 μM Pd^{2+} vs. 4 nM Au NPs) and enough Pt^{2+} (such as 600 μM Pt^{2+}) in the reaction solution, the molar ratio of Pt/Au in the produced Au@PdPt NPs was calculated to be 7.67%. That is, the Pt content is only slightly less than that of Au@Pt NPs and 1.12 Pt layers were deposited on Au core. With further adding enough Pd^{2+} ions (such as 600 μM), the molar ratio of Pt/Au in Au@PdPt NPs was measured to be 8.22%, corresponding to 1.20 Pt layers on the Au core. These results clearly indicate that there is basically constant Pt content in the shell of Au@PdPt NPs and Au@Pt NPs in spite of the addition of different amounts of Pd^{2+}. On the other hand, the Pd content in the shells of Au@PdPt NPs increases with the increase of Pd dosage. In addition, for other three samples of Au@PdPt NPs with less than a Pt monolayer, with the decrease of Pt content in the shell of Au@PdPt NPs, the Pd content continues to increase.

It should be pointed out that based on the mechanism of Au catalytic reduction catalysis, the formed PdPt shell in the Au@PdPt NPs has a limited layer thickness [32]. As shown in Table S1, up to about 2.6 atomic PdPt layers can be formed on the surface of Au core. Under the present experimental conditions, the molar ratios of Pd/Pt were calculated and presented in Table S1. To distinguish these nanoparticles, the samples were named as Au@$Pd_{0.31}Pt_1$, Au@$Pd_{0.61}Pt_1$, Au@$Pd_{0.86}Pt_1$, Au@$Pd_{1.19}Pt_1$, Au@$Pd_{1.81}Pt_1$, Au@$Pd_{2.18}Pt_1$ and Au@$Pd_{4.20}Pt_1$ NPs, corresponding to 1.12, 1.13, 1.15, 1.20, 0.91, 0.82, and 0.50 Pt atomic layers on Au surface, respectively.

Since the sample of Au@$Pd_{1.19}Pt_1$ NPs showed the highest catalytic activity for ORR, its structure was studied in detail. The size and morphology of Au and Au@$Pd_{1.19}Pt_1$ NPs were first characterized by transmission electron microscopy (TEM). As shown in Figure S1 (Supporting Information online), citrate-stabilized Au NPs are spherical and monodispersed with the average diameter of 14.12±0.54 nm. By comparison, the prepared Au@$Pd_{1.19}Pt_1$ NPs also show similar spherical morphology with the average diameter of 15.08±0.61 nm (Figure 1(a)). The unobvious size change suggests that an ultrathin PdPt metal shell (<1 nm) covers on the surface of Au NPs. The surface lattices of the produced nanoparticles were investigated and the high-resolution TEM images are shown in Figure S2 and Figure 1(b). The surface of the nanoparticles is covered by Au (111) crystal plane with interplanar spacing of 2.36 Å. Such surface structure suggests that no new crystal lattice is formed after the formation of PdPt skin on the surface of Au NPs, which demonstrates again the ultrathin PdPt shell formed on the gold nanoparticle core.

To further study the distributions of Pd, Pt and Au in the Au@$Pd_{1.19}Pt_1$ NPs, the energy-dispersive X-ray spectroscopy (EDX) analysis was carried out. The EDX spectrum shown in Figure S3 demonstrates that the Au@$Pd_{1.19}Pt_1$ NPs

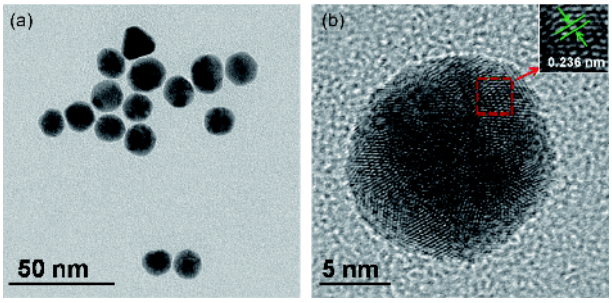

Figure 1 TEM (a) and high-resolution TEM (b) images of Au@$Pd_{1.19}Pt_1$ NPs (color online).

have a substantially high Au content with only a small amount of Pd and Pt. The line scanning profile across a single Au@$Pd_{1.19}Pt_1$ NP shows a main distribution of Au in the core and the uniform distributions of Pd and Pt in the shell with very low content (Figure 2(a)). The analysis of high-angle annular dark-field scanning transmission electron microscopy (HAADF-STEM) for Au@$Pd_{1.19}Pt_1$ NPs is shown in Figure 2(b–f). It can be seen that only small amounts of Pt and Pd elements are dispersed on the surface of Au core with a uniform distribution, suggesting the formation of Au@$Pd_{1.19}Pt_1$ core@shell structured NPs with a thin PdPt-skin surface.

The crystal structures of the prepared nanoparticles were studied by the powder X-ray diffraction (XRD), as shown in Figure 3. All the samples show similar face-centered cubic (fcc) crystal structure and the XRD patterns are consistent well with the standard diffraction spectrum of Au (marked as black bars). However, the fcc crystal diffraction signals from Pd (marked as red bars) and Pt (marked as blue bars) cannot be observed. Such data suggest that the ultrathin PdPt shell cannot form a new crystal surface, which agrees well with the above EDX and TEM characterizations.

The XPS measurements were carried out to examine the chemical states of Pd and Pt in the Au@$Pd_{1.19}Pt_1$ NPs. In the wide-scan XPS survey spectrum (Figure S4), the signals of Au 4f, Pd 3d and Pt 4f can be observed obviously. The high resolution XPS spectra of Pd 3d, Pt 4f and Au 4f are shown in Figures 4 and S5, respectively. In the Pd 3d spectrum, the two characteristic peaks (334.32 and 339.50 eV) correspond to the binding energies of Pd^0 (Figure 4(a)). Moreover, as shown in Figure 4(b), in the Pt 4f spectrum, the two characteristic peaks (70.07 and 73.44 eV) correspond to the binding energies of Pt^0. The XPS results confirm the zero valences of Pd and Pt in the Au@$Pd_{1.19}Pt_1$ NPs. Meanwhile, compared to the Pd 3d peaks of 337.55 and 342.84 eV from Pd/C catalyst and Pt 4f peaks of 71.05 and 74.27 eV from Pt/C catalysts (Figure 4(c, d)), there present negative shifts of the binding energies for Pd and Pt in the Au@$Pd_{1.19}Pt_1$ NPs, indicating that the charge transfer occurs from Au core to the PdPt shell.

3.3 Electrocatalytic activity of the trimetallic Au@PdPt core-shell nanoparticles for oxygen reduction reaction (ORR)

The electrochemical properties of the synthesized nanoparticles were firstly investigated by voltammetric measurements in 0.1 M $HClO_4$ solution. The four Au@PdPt samples with more than one Pt monolayer (the molar ratios of Pd/Pt are 0.31, 0.61, 0.86 and 1.19, respectively) were firstly studied and the cyclic voltammograms (CVs) are shown in Figure 5(a) (in N_2-saturated electrolyte) and Figure S6 (in O_2-saturated electrolyte), respectively. The results clearly indicate that with increasing the Pd content in these Au@PdPt NPs, the currents from the hydrogen adsorption/desorption increase obviously. Meanwhile, the current peaks from the reduction of metal oxides in N_2 atmosphere and the oxygen reduction in O_2 atmosphere are notably enhanced. These results indicate that the Au@$Pd_{1.19}Pt_1$ NPs (black curve in Figures 5(a) and S6) present the highest electro-

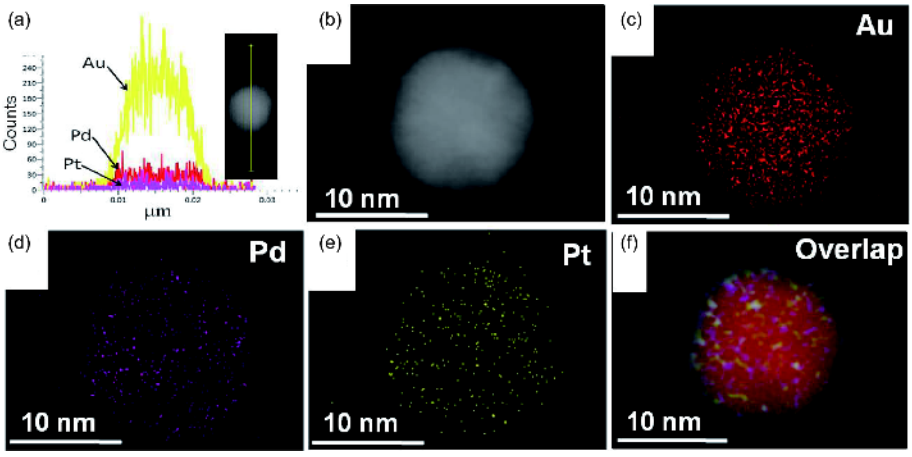

Figure 2 (a) Line-scanning profile across a single Au@$Pd_{1.1}$9Pt_1 NP; (b) HAADF-STEM image of Au@$Pd_{1.19}Pt_1$ NPs; elemental mapping images of Au (c), Pd (d), Pt (e) and their overlap (f) (color online).

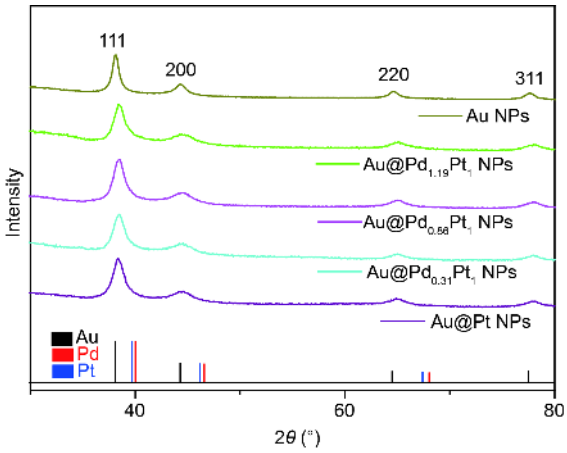

Figure 3 XRD patterns of the Au, Au@PdPt, and Au@Pt NPs. black, red and blue bars indicate the positions of diffraction peaks from the standard Au (JCPDS 65-2870), Pd (JCPDS 65-2867) and Pt (JCPDS 65-2868), respectively (color online).

chemical catalytic activity among the synthesized Au@PdPt NPs because of the maximum Pd content in the PdPt shell. Subsequently, the corrosion resistance of the Au@Pt NPs and Au@PdPt NPs in acid solution was studied with setting the upper potential limit at 1.6 V (vs. Ag/AgCl). As shown in Figure S7, multiple CV cycles of the Au@Pt NPs were recorded at the scan rate of 100 mV s^{-1}. For the first cycle (red curve), in the negative potential scanning there is no obvious current peak from the reduction of Au oxide, which suggests that the Au cores are initially completely covered with the Pt-skin shell (1.22 Pt monolayers on Au core calculated in Table S1). However, from the second cycle, the current peak from the reduction of Au oxide appears and increases gradually; and meanwhile, the reduction peak from the Pt oxides decreases obviously. These results suggest that the Au@Pt NPs are unstable in acid solution without the protection of Pd-contained shell. By contrast, after the multiple CV treatment in the same potential range (−0.2–1.6 V, vs. Ag/AgCl), obvious current peaks (at 0.2–0.4 V vs. Ag/AgCl) from the reduction of PdPt oxides can be observed for the four Au@PdPt NPs (Figure S8). Furthermore, the CV from $Au@Pd_{1.19}Pt_1$ NPs presents no current peak from the reduction of Au oxide. However, the CVs from other three samples of Au@PdPt NPs show distinct Au oxide reduction peaks at 0.8 V (vs. Ag/AgCl). According to the calculation data shown in Table S1, the surface of Au core could be almost fully covered with the PdPt shell in these particles. Based on these results, in the low-pH media, for the Au@PdPt NPs with more than one monolayer of Pt, more Pd content in the PdPt shell can effectively protect the Pt-skin surface and thus improve the electrochemical stability of the Au@PdPt NPs.

Then, with further increasing the Pd content, the electrochemical properties of the obtained three Au@PdPt samples with less than one monolayer of Pt in PdPt shell (the molar ratios of Pd/Pt are 1.81, 2.18 and 4.20, respectively) were studied. From the CV curves shown in Figures S9–S11, these core@shell nanoparticles are unstable in 0.1 M $HClO_4$ solution. In the scanning process of multiple CV cycles, both the hydrogen absorption/desorption and the oxygen reduction peaks of the three samples all increase first and then decrease significantly. We speculate that the reasons are as

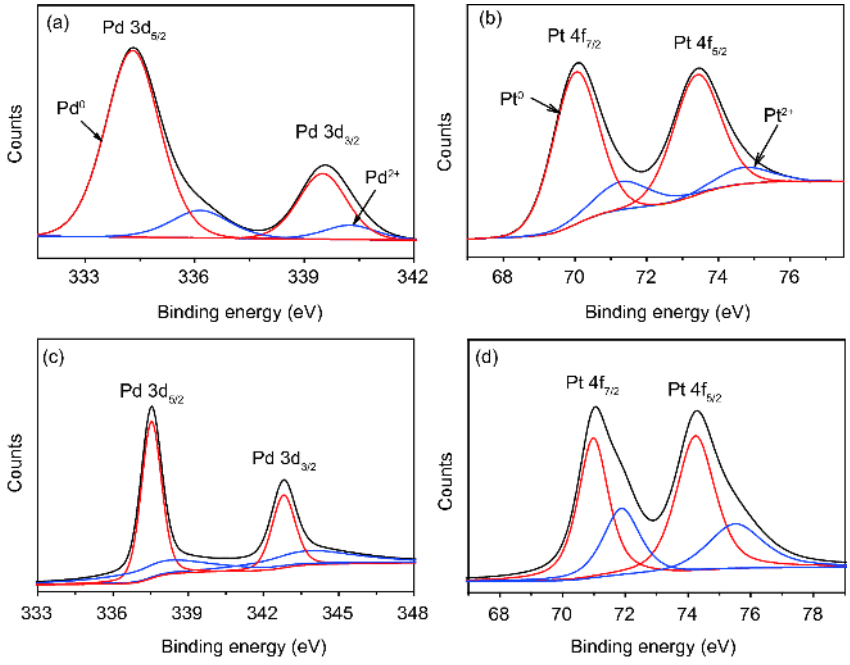

Figure 4 High-resolution XPS spectra of Pd 3d (a) and Pt 4f (b) in the $Au@Pd_{1.19}Pt_1$ NPs; Pd 3d spectrum of the Pd/C catalyst (c) and Pt 4f spectrum of the Pt/C catalyst (d) (color online).

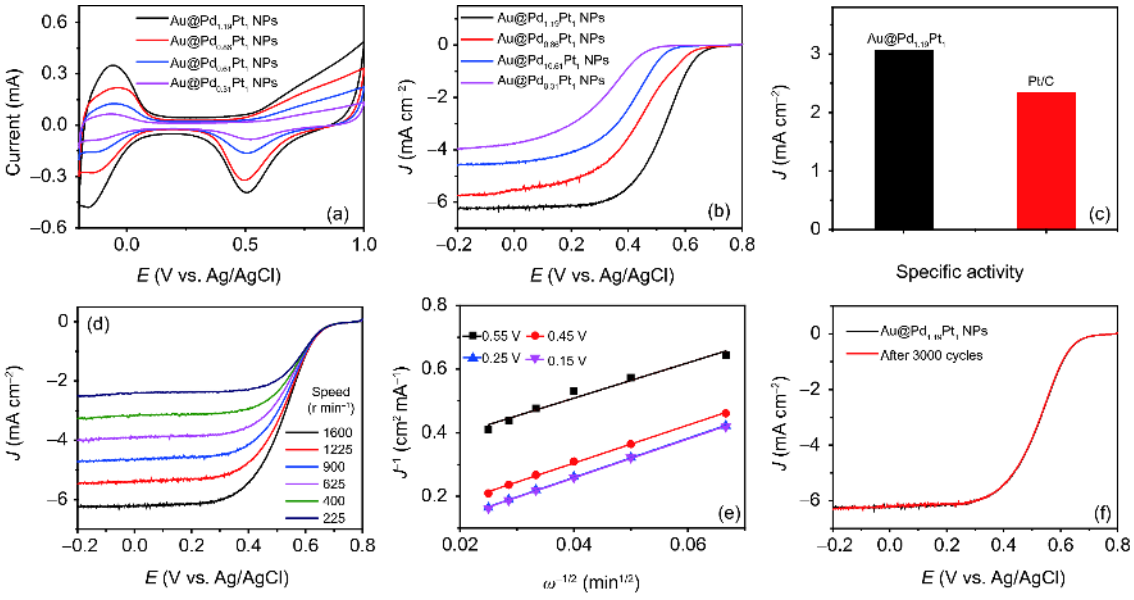

Figure 5 (a) CVs of various Au@PdPt NPs with different Pd contents in N_2-saturated 0.1 M $HClO_4$ solution with 50 mV s^{-1}; (b) ORR polarization curves of the Au@PdPt NPs in 0.1 M O_2-saturated $HClO_4$ solution with a rotation rate of 1600 r min^{-1} at 10 mV s^{-1}; (c) specific kinetic current densities of ORR on $Au@Pd_{1.19}Pt_1$ NPs and commercial Pt/C at 0.528 V (vs. Ag/AgCl); (d) ORR polarization curves of $Au@Pd_{1.19}Pt_1$ NPs in O_2-saturated 0.1 M $HClO_4$ solution at a scan rate of 10 mV s^{-1}; (e) Koutecky-Levich plots (J^{-1} vs. $\omega^{-1/2}$) from $Au@Pd_{1.19}Pt_1$ NPs at different potentials (vs. Ag/AgCl); (f) polarization curves of the $Au@Pd_{1.19}Pt_1$ NPs before and after 3000 potential cycles in 0.1 M O_2-saturated $HClO_4$ solution with a potential range from 0.1 to 0.7 V (vs. Ag/AgCl) (color online).

follows. In the Au@PdPt NPs, Pd in PdPt layer can compensate the consumption of Pt during the electrochemical reactions in acid medium. Meanwhile, no less than a Pt monolayer is also necessary on the outermost surface, because the closely arranged Pt atoms on the surface can slow down the dissolution of Pd. Due to the more inert property of Au core than Pd and Pt, if Pt on the surface is less than a single layer, part of Pd will be exposed, which may accelerate the dissolution of Pd and quickly lose the protection for Pt. Based on these reasons, the electrochemical properties of these particles are not stable under acidic conditions.

Therefore, for the synthesis of Au@PdPt NPs by the Au catalytic reduction strategy, slightly more than one single layer of Pt and meanwhile more Pd content in the shell are necessary for their application in electrocatalysis with satisfactory high stability. Based on these results, the $Au@Pd_{1.19}Pt_1$ is the optimal structure in the synthesized core@shell samples.

Because of the unstable electrochemical properties of Au@PdPt NPs with less than one monolayer of Pt in PdPt shell, the four samples of $Au@Pd_{0.31}Pt_1$, $Au@Pd_{0.61}Pt_1$, $Au@Pd_{0.86}Pt_1$ and $Au@Pd_{1.19}Pt_1$ NPs are mainly studied below. The ORR polarization curves of these Au@PdPt NPs and commercial Pt/C catalyst were recorded in O_2-saturated $HClO_4$ solution with the rotation rate of 1600 r min^{-1}. As shown in Figure 5(b) and Figure S12, clearly, the $Au@Pd_{1.19}Pt_1$ NPs have the more positive onset potential and half-wave potential for ORR than other Au@PdPt NPs and Pt/C catalyst. The specific and mass activities of these core@shell nanparticles were calculated at 0.528 V (the half wave potential of $Au@Pd_{1.19}Pt_1$ NPs). The specific activity of $Au@Pd_{1.19}Pt_1$ NPs is 3.06 mA cm^{-2} (shown in Figure 5(c)), which is not only 1.31 times higher than that of Pt/C catalyst (2.32 mA cm^{-2}), but also much higher than those of other Au@PdPt NPs (Figure S13). In addition, as shown in Figure S14, the mass activity of $Au@Pd_{1.19}Pt_1$ NPs is 598.53 mA mg_{pt}^{-1}, which is about 6.1 times larger than that of the Pt/C catalyst (98.30 mA mg_{pt}^{-1}). Based on above results, in a wide rotation rate range, the ORR polarization curves on the $Au@Pd_{1.19}Pt_1$ NPs were measured (Figure 5(d)), from which the Koutecky-Levich plots were then obtained (shown in Figure 5(e)). From the slopes of the K-L plots, 3.9 electrons are involved per oxygen reduction, suggesting a nearly four-electron pathway for the reduction of oxygen to water with $Au@Pd_{1.19}Pt_1$ NPs as catalysts [35].

Furthermore, accelerated durability tests (ADTs) were measured in 0.1 M $HClO_4$ solution with a cycling potential range from 0.1 to 0.7 V (vs. Ag/AgCl). Before and after 3000 potential cycles, the polarization curves from the $Au@Pd_{1.19}Pt_1$ NPs and Pt/C catalyst for ORR are shown in Figures 5(f) and S15, respectively. The experimental results show that after the ADTs, the polarization curve of ORR is almost unchanged on the $Au@Pd_{1.19}Pt_1$ NPs (Figure 5(f)). However, ORR polarization curve on commercial Pt/C presents an obvious change (Figure S12). The above data illustrate that the $Au@Pd_{1.19}Pt_1$ NPs have much higher electrochemical stability and enhanced activity than the commercial Pt/C for ORR in acid electrolyte.

4 Conclusions

In summary, a series of trimetallic Au@PdPt core@shell nanoparticles with different Pd contents in the shell were synthesized by the Au catalytic reduction strategy and subsequent metal replacement reaction. The prepared Au@PdPt NPs consist of 14 nm Au core in diameter and an ultrathin PdPt-skin surface. In these Au@PdPt NPs, the $Au@Pd_{1.19}Pt_1$ NPs showed the higher electrocatalytic activity and stability for ORR in acid solution than other Au@PdPt NPs and Pt/C catalyst. The superior performance could be attributed to introducing Pd into the shell of Au-Pt nanostructures which can effectively prevent the dissolution of Pt in acid solution and then guarantee the electrochemical activities of platinum-based nanomaterials. The present work demonstrates that the Au@PdPt nanostructures with an ultrathin bimetallic PtPd-skin surface have a potential application in fuel cells as advanced cathodic electrocatalysts.

Acknowledgements This work was supported by the National Natural Science Foundation of China (21773224, 21633008, 21575134, 11374297, 21405149), the National Key Research and Development Plan (2016YFA0203200) and K. C. Wong Education Foundation.

Conflict of interest The authors declare that they have no conflict of interest

Supporting information The supporting information is available online at http://chem.scichina.com and http://link.springer.com/journal/11426. The supporting materials are published as submitted, without typesetting or editing. The responsibility for scientific accuracy and content remains entirely with the authors.

1 Shao M, Chang Q, Dodelet JP, Chenitz R. *Chem Rev*, 2016, 116: 3594–3657
2 Chen A, Holt-Hindle P. *Chem Rev*, 2010, 110: 3767–3804
3 Kang Y, Snyder J, Chi M, Li D, More KL, Markovic NM, Stamenkovic VR. *Nano Lett*, 2014, 14: 6361–6367
4 Wang C, Markovic NM, Stamenkovic VR. *ACS Catal*, 2012, 2: 891–898
5 Wang C, Chi M, Li D, Strmcnik D, van der Vliet D, Wang G, Komanicky V, Chang KC, Paulikas AP, Tripkovic D, Pearson J, More KL, Markovic NM, Stamenkovic VR. *J Am Chem Soc*, 2011, 133: 14396–14403
6 Sasaki K, Naohara H, Choi YM, Cai Y, Chen WF, Liu P, Adzic RR. *Nat Commun*, 2012, 3: 1115
7 He LL, Zheng JN, Song P, Zhong SX, Wang AJ, Chen Z, Feng JJ. *J Power Sources*, 2015, 276: 357–364
8 Wang G, Huang B, Xiao L, Ren Z, Chen H, Wang D, Abruña HD, Lu J, Zhuang L. *J Am Chem Soc*, 2014, 136: 9643–9649
9 Dai Y, Chen S. *ACS Appl Mater Interfaces*, 2015, 7: 823–829
10 Hunt ST, Milina M, Alba-Rubio AC, Hendon CH, Dumesic JA, Román-Leshkov Y. *Science*, 2016, 352: 974–978
11 Shi G, Yano H, Tryk DA, Iiyama A, Uchida H. *ACS Catal*, 2017, 7: 267–274
12 Lu Y, Jiang Y, Chen W. *Nano Energy*, 2013, 2: 836–844
13 Sun X, Li D, Ding Y, Zhu W, Guo S, Wang ZL, Sun S. *J Am Chem Soc*, 2014, 136: 5745–5749
14 Guo S, Zhang S, Su D, Sun S. *J Am Chem Soc*, 2013, 135: 13879–13884
15 Zhang S, Guo S, Zhu H, Su D, Sun S. *J Am Chem Soc*, 2012, 134: 5060–5063
16 Barman SC, Hossain MF, Yoon H, Park JY. *Biosens Bioelectron*, 2018, 100: 16–22
17 Wang L, Yamauchi Y. *J Am Chem Soc*, 2010, 132: 13636–13638
18 Venarusso LB, Bettini J, Maia G. *J Solid State Electrochem*, 2016, 20: 1753–1764
19 Wang C, van der Vliet D, More KL, Zaluzec NJ, Peng S, Sun S, Daimon H, Wang G, Greeley J, Pearson J, Paulikas AP, Karapetrov G, Strmcnik D, Markovic NM, Stamenkovic VR. *Nano Lett*, 2011, 11: 919–926
20 Wang Q, Chen S, Shi F, Chen K, Nie Y, Wang Y, Wu R, Li J, Zhang Y, Ding W, Li Y, Li L, Wei Z. *Adv Mater*, 2016, 28: 10673–10678
21 Zeng J, Yang J, Lee JY, Zhou W. *J Phys Chem B*, 2006, 110: 24606–24611
22 Zhang J, Sasaki K, Sutter E, Adzic RR. *Science*, 2007, 315: 220–222
23 Mourdikoudis S, Chirea M, Zanaga D, Altantzis T, Mitrakas M, Bals S, Liz-Marzán LM, Pérez-Juste J, Pastoriza-Santos I. *Nanoscale*, 2015, 7: 8739–8747
24 Li D, Meng F, Wang H, Jiang X, Zhu Y. *Electrochim Acta*, 2016, 190: 852–861
25 Chen A, Ostrom C. *Chem Rev*, 2015, 115: 11999–12044
26 Lim B, Jiang M, Camargo PHC, Cho EC, Tao J, Lu X, Zhu Y, Xia Y. *Science*, 2009, 324: 1302–1305
27 Sasaki K, Naohara H, Cai Y, Choi YM, Liu P, Vukmirovic MB, Wang JX, Adzic RR. *Angew Chem Int Ed*, 2010, 49: 8602–8607
28 Fang PP, Duan S, Lin XD, Anema JR, Li JF, Buriez O, Ding Y, Fan FR, Wu DY, Ren B, Wang ZL, Amatore C, Tian ZQ. *Chem Sci*, 2011, 2: 531–539
29 Duan S, Ji YF, Fang PP, Chen YX, Xu X, Luo Y, Tian ZQ. *Phys Chem Chem Phys*, 2013, 15: 4625–4633
30 Liu CW, Wei YC, Liu CC, Wang KW. *J Mater Chem*, 2012, 22: 4641–4644
31 Huang X, Zhang H, Guo C, Zhou Z, Zheng N. *Angew Chem Int Ed*, 2009, 48: 4808–4812
32 Zhang Y, Li X, Li K, Xue B, Zhang C, Du C, Wu Z, Chen W. *ACS Appl Mater Interfaces*, 2017, 9: 32688–32697
33 Turkevich J, Stevenson PC, Hillier J. *Discuss Faraday Soc*, 1951, 11: 55–75
34 Frens G. *Nat Phys Sci*, 1973, 241: 20–22
35 Lu Y, Wang Y, Chen W. *J Power Sources*, 2011, 196: 3033–3038